International Journal of Numerical Methods for Heat & Fluid Flow

Analysis of freezing process about falling droplet using the lattice Boltzmann method

Xin Zhao, Bo Dong, Weizhong Li,

Analysis of the freezing process about a falling droplet using the lattice Boltzmann method

Xin Zhao, Bo Dong and Weizhong Li
School of Energy and Power Engineering, Dalian University of Technology, Dalian, China

Received 19 September 2017
Revised 19 January 2018
Accepted 3 February 2018

Abstract

Purpose – The freezing phenomenon of a falling droplet is a frequently encountered phenomenon in various applications, such as spray crystallization, hail formation and artificial snowmaking. Therefore, this paper aims to understand the freezing processes of a falling droplet without and with initial horizontal velocity in a cold space.

Design/methodology/approach – The freezing processes of a falling droplet were characterized using a modified enthalpy-based lattice Boltzmann method.

Findings – The temperature field, streamlines and freezing process of the falling droplet were investigated and analyzed. The lower part of the droplet was frozen earlier than the upper part. The freezing trend slowed down in the later stage of the freezing process. The droplet shape was related to the initial vertical velocity, nucleation temperature and initial horizontal velocity.

Originality/value – A modified enthalpy-based lattice Boltzmann method is proposed. In the model, the improved pseudo-potential model is used and the radiation is considered. This method was firstly used to simulate the freezing process of a falling droplet. By examining these freezing processes in detail, the freezing trend and the effect factors of droplet deformation and freezing time were obtained, respectively.

Keywords Phase change, Lattice Boltzmann method, Droplet, Falling, Freezing trend

Paper type Research paper

Nomenclature

A = surface area of the droplet (m^2);
C = coefficient;
c = lattice speed;
C_p = liquid specific heat capacity ($J/(kg \cdot K)$);
C_s = lattice speed of sound;
c_{solid} = solid specific heat capacity ($J/(kg \cdot K)$);
D = droplet diameter (m);
$\mathbf{e}_i$ = discretized velocity in the ith direction;
$\mathbf{F}$ = total force (N);
$\mathbf{F}f$ = interaction force between particles (N);
$\mathbf{F}_g$ = gravitational force (N);
$f(x^*)$ = interface curve function;

International Journal of Numerical Methods for Heat & Fluid Flow
Vol. 28 No. 10, 2018
pp. 2442-2462

0961-5539
DOI 10.1108/HFF-09-2017-0373

The work was jointly sponsored by the National Science Foundation of China (NSFC) under Grant No. 51776031, the key program of National Science Foundation of Liaoning Province under Grant No. 20170540182 and the Fundamental Research Funds for the Central Universities under Grant No. DUT16QY03.

f_i = particle distribution function before collision;
f_i^* = particle distribution function after collision;
$f_i^{(eq)}$ = equilibrium particle distribution function;
G = interaction strength between the phases;
$G(\mathbf{x},\mathbf{x}')$ = Green's function;
g_i = particle distribution function before collision;
$g_i^{(eq)}$ = equilibrium particle distribution function;
g = gravitational acceleration (m/s^2);
H = enthalpy (J);
H_b = beginning enthalpy (J);
H_e = ending enthalpy (J);
I = intensity (W/sr);
I_i = particle distribution function before collision;
$I_i^{(eq)}$ = equilibrium particle distribution function;
i = direction;
k = thermal conductivity ($W/(m \cdot K)$);
L = latent heat (J/kg);
L_s = latent heat of freezing of water (J/kg);
m = coefficient;
$\bar{q}_R$ = radiative heat flux (W);
$T*$ = dimensionless initial temperature (K);
T_{bound} = boundary temperature (K);
$T_{g,in}$ = initial cold space temperature (K);
$T_{l,in}$ = initial droplet temperature (K);
T_n = nucleation temperature (K);
t = time (s);
$\mathbf{u}$ = velocity (m/s);
v_0 = initial vertical velocity (m/s);
v_h = initial horizontal velocity (m/s);
W_D = total weight of the droplet (kg);
W_s = weight of ice in the droplet (kg);
$\mathbf{W}_i$, w_{gi} = weighted coefficient;
$\mathbf{X}$ = position on the lattice;
x^* = dimensionless coordinate; and
x_0^* = intersection of line $y^* = x^*$ and interface curve in x^*, y^* domain.

Greek symbols

α_s = solid volume fraction;
β = ratio of latent heat to sensible heat;
δ_i = azimuthal angle;
δ_t = time step;
η = integration variable;
Λ = dimensionless constant;
λ_0 = constant;
v = kinematic viscosity (m^2/s);
σ_{SB} = Stefan-Boltzmann constant ($W/m^3 \cdot K^4$);
ρ = density (kg/m^3);
ρ_l = droplet density (kg/m^3);
τ = relaxation time;

τ_0 = integration variable;
τ_i = relaxation time for intensity;
τ_T = relaxation time for temperature field;
ψ = effective density; and
ω_i = weighted coefficient.

1. Introduction

The problem about the freezing process of a falling droplet in a cold space has received increasing attention, owing to the widespread applications in many fields, such as artificial snowmaking, hail formation, cryogenic storage and spray crystallization (Hindmarsh *et al.*, 2007; Nagumo and Fujiyoshi, 2015; Gao *et al.*, 2016). When the droplet temperature is below the freezing point, the droplet is frozen during its falling process. In the past several decades, the freezing process of a falling droplet has been widely investigated by theoretical, experimental and numerical studies. Hobbs and Alkezweeny (1968) provided some theoretical expressions to calculate the degree at which a droplet falls through a gas at a vertical temperature gradient. Miller *et al.* (1976) worked out an empirical expression of the homogeneous ice nucleation. Jeffery and Austin (1997) proposed some new theoretical estimates for the homogeneous nucleation rate based on a new analytic state equation. However, it should be noted that the theoretical analysis has a large limitation in the accuracy of calculation due to solving the nonlinear equations.

The evolution of the freezing process has attracted a great deal of interest for many years. The main finding of the experimental work is that the application of polarized light (Hallett, 1964), scattered light from a He–Ne laser (Krämer *et al.*, 1999), magnetic resonance imaging (MRI) (Hindmarsh *et al.*, 2004) and ultrasonic atomizer (López and Ávila, 2012). For the sake of precision and reproducibility, microscopic observation has become a powerful method for many experiments. Huang and Bartell (1995) used the electron diffraction measurement at microsecond intervals to establish the presence of liquid water at T = −70°C and then obtained the nucleation rate. However, it should be admitted that either theoretical analyses or experimental studies about the freezing process of a falling droplet is still a challenging issue. The difficulty is mainly caused by the irregular evolution of the moving solid–liquid interface, the complex microstructure of the solid–liquid region, as well as the temperature field. Additionally, the precision of the equipment has a great effect on the experiment results. For instance, in the condition of humidity higher than 90 per cent and surface temperature at –25°C, some white smoke is observed near the cold surface. It is essentially the tiny water droplets formed by condensation of water vapor in the size of micron scale. It is difficult to track the trajectory of a particular droplet, and even using a magnification of 225 times. It is still unable to observe the morphological change of this continuous movement of the droplet. Similarly, it is also hard to measure the solid–liquid interface in a droplet to judge whether it has been frozen before it reaches the cold surface.

Because of the wide variety of physical problems exhibiting the phase change phenomenon, numerous scientists are attracted to the freezing field and investigations in this area are now very active. Wood *et al.* (2002) used a standard Maxwell-type model for modeling the homogeneous and heterogeneous ice nucleation in free-falling water droplets. For the traditional CFD methods, Anandharamakrishnan *et al.* (2009) applied a finite volume method to simulate the behavior of spray-freezing. However, the approach based on the finite volume scheme brings large computation costs. The accuracy of the simulation results not only depends on the establishment of the mathematical model, but also on the computational grid. As an effective numerical tool for computational fluid dynamics, the

lattice Boltzmann method (LBM) has been successfully used to simulate the phase change problem (Zarghami *et al.*, 2014; Du *et al.*, 2017). The LBM has the attractive advantages on numerical stability, constitutive versatility and validity of fluid flow and heat/mass transfer application involving interfacial dynamics and complex boundary conditions. In terms of the phase change problem, there are mainly two kinds of LBMs: one is phase-field method (Miller *et al.*, 2006) and the other is enthalpy-based method (Jiaung *et al.*, 2001). To reproduce the dynamics of the sharp interface equation, the phase-field method requires an extremely finer grid to resolve the interfacial region in principle. Thus, the enthalpy-based LBM is chosen in the present study. It is not necessary to use finer grid spacing in the interface region because the interface width in this model can be theoretically limited to one grid spacing for the isothermal phase change problems. Jiaung *et al.* (2001) proposed an enthalpy-based LBM to simulate the non-isothermal phase change problem. However, the impact of the freezing process on the fluid flow is not considered in solving the freezing process involving fluid flow. Therefore, an improved enthalpy-based LBM was developed (Zhao *et al.*, 2017). The solid volume fraction was used to modify the migration process of the evolution equation.

In this study, a modified enthalpy-based LBM is proposed. In the present model, the improved pseudo-potential model is used to calculate the inter-particle interaction force for ensuring the conservation of the total momentum of system. Additionally, the radiation is considered due to the relatively large temperature difference. The solid volume fraction is used to modify the migration process of the evolution equation for solving the non-isothermal phase change problem. Then, the modified model is used to investigate the freezing processes of a falling droplet without and with initial horizontal velocity, respectively. The following part of this article is organized as follows. First, a modified enthalpy-based LBM is briefly introduced in Section 2. Second, the freezing process of a falling droplet in a cold space is simulated in Section 3. In Section 4, the freezing process of a falling droplet with initial horizontal velocity is investigated. Finally, the conclusions are made in Section 5.

2. A modified enthalpy-based lattice Boltzmann model

When the freezing process of a falling droplet is studied, as the freezing goes, latent heat is released at the solid–liquid interface, which results in thermal gradient ahead of the interface. During the freezing process, a solid shell formed at the droplet surface is assumed to be rigid and stationary. The fluid flow is hindered by the solid shell, but the heat transfer continues. This interaction of thermal transport and solid shell growth does not stop until the end of freezing process. In this study, a modified enthalpy-based LBM is used to investigate this problem.

The evolution equation of particle distribution function is:

$$f_i(\mathbf{x}+\mathbf{e}_i\delta_t, t+\delta_t) = f_i(\mathbf{x},t) - \frac{1}{\tau}\left[f_i(\mathbf{x},t) - f_i^{(eq)}(\mathbf{x},t)\right] \tag{1}$$

where f is the particle distribution function. x is the position on the lattice. t is the time. δ_t is the time step. τ is the relaxation time.

Flow field is dispersed by the D2Q9 model. The discrete velocity in the ith direction is:

$$\mathbf{e}_i = \begin{cases} (0,0), & i=0; \\ (\pm 1,0)c, \quad (0,\pm 1)c, & i=1,2,3,4; \\ (\pm 1,\pm 1)c, & i=5,6,7,8. \end{cases} \tag{2}$$

where c is the lattice speed.

The corresponding equilibrium particle distribution function $f_i^{(eq)}(\mathbf{x}, t)$ is:

$$f_i^{(eq)} = \omega_i \rho \left[1 + \frac{\mathbf{e}_i \cdot \mathbf{u}^{\mathbf{eq}}}{{c_s}^2} + \frac{(\mathbf{e}_i \cdot \mathbf{u}^{\mathbf{eq}})^2}{2{c_s}^4} - \frac{\mathbf{u}^{\mathbf{eq}} \cdot \mathbf{u}^{\mathbf{eq}}}{2{c_s}^2} \right] \tag{3}$$

where the lattice speed of sound is $c_s = c/\sqrt{3}$. The kinetic viscosity is $\nu = (\tau\text{-}0.5){c_s}^2 \delta_t$. The weighted coefficients ω_i are:

$$\omega_i = \begin{cases} 4/9 & i = 0 \\ 1/9 & i = 1, \ldots, 4 \\ 1/36 & i = 5, \ldots, 8 \end{cases} \tag{4}$$

In the improved pseudo-potential model, it assumes that the nonlocal interaction exist between the fluid particles (Shan and Chen, 1994). The inter-particle interaction force is:

$$\mathbf{F}_f(\mathbf{x}) = -\psi(\mathbf{x}) \sum_{\mathbf{x}'} G(\mathbf{x}, \mathbf{x}) \psi(\mathbf{x})(\mathbf{x} - \mathbf{x}) \tag{5}$$

where $G(\mathbf{x}, \mathbf{x}') = \begin{cases} G, & \mathbf{e}_i = c; \\ G/4, & \mathbf{e}_i = \sqrt{2}c; \\ 0, & otherwise. \end{cases}$ is the Green's function. The interaction strength between the phases is decided by the absolute value of G. The effective density is $\psi(\rho) = \rho^*[1 - \exp(\rho/\rho^*)]$.

The gravitational force is:

$$\mathbf{F}_g(\mathbf{x}) = \rho(\mathbf{x}) g \tag{6}$$

where g is gravitational acceleration. The total force is $\mathbf{F(x)} = \mathbf{F}_f\mathbf{(x)} + \mathbf{F}_g\mathbf{(x)}$.

The equilibrium velocity $\mathbf{u}^{eq}$ is:

$$\mathbf{u}^{eq} = \mathbf{u}(\mathbf{x}, t) + \tau \delta_t \frac{\mathbf{F}(\mathbf{x})}{\rho} \tag{7}$$

The solid volume fraction α_s is:

$$\alpha_s = \begin{cases} 0, & H > H_b \\ \dfrac{H - H_e}{H_b - H_e}, & H_b \leq H \leq H_e \\ 1, & H < H_e \end{cases} \tag{8}$$

The enthalpy value H is:

$$H = \alpha_s c_{solid} T + (1 - \alpha_s) c_p T + \alpha_s L \tag{9}$$

Particularly, $H_b = c_p T_b$ for $\alpha_s = 0$ and $H_e = c_{solid} T_e + L$ for $\alpha_s = 1$ are the beginning enthalpy and the ending enthalpy of freezing process, respectively. T_e is the ending temperature and

T_b is the beginning temperature which is equal to the nucleation temperature T_n. c_{solid} and c_p are the solid and liquid specific heat capacity, respectively. The latent heat L is considered at the solid–liquid surface.

In this model, the radiation is considered. Using the BGK approximation, the evolution equation of particle distribution function g_i for simulating the temperature field is:

$$g_i(\mathbf{x}+\mathbf{e}_i\delta_t, t+\delta_t) = g_i(\mathbf{x},t) - \frac{1}{\tau_T}\left[g_i(\mathbf{x},t) - g_i^{eq}(\mathbf{x},t)\right] - \omega_i\delta_t\frac{L}{c_p}\left[\frac{\alpha_s(\mathbf{x},t+\delta_t)-\alpha_s(\mathbf{x},t)}{\delta_t}\right] - \omega_i\delta_t\frac{\nabla\cdot\overline{q}_R}{\rho c_p} \tag{10}$$

where g_i is the particle distribution function, τ_T is the relaxation time. The corresponding equilibrium particle distribution function $g_i^{(eq)}(\mathbf{x},t)$ is:

$$g_i^{(eq)} = \omega_i T\left[1+\frac{\mathbf{e}_i\cdot\mathbf{u}}{{c_s}^2}+\frac{(\mathbf{e}_i\cdot\mathbf{u})^2}{2{c_s}^4}-\frac{\mathbf{u}\cdot\mathbf{u}}{2{c_s}^2}\right] \tag{11}$$

The radiative heat flux $\vec{q}_R = \sum_{i=1}^{Q} I_i\mathbf{w}_i$ is calculated by the lattice Boltzmann formulation (Asinari *et al.*, 2010). Here, I_i is the intensity. $\mathbf{w}_i = \left(\pi\cos\delta_i\sin\left(\frac{\Delta\delta_i}{2}\right), \pi\sin\delta_i\sin\left(\frac{\Delta\delta_i}{2}\right)\right)$ is the weighted coefficient. The evolution equation for calculating the intensity is:

$$I_i(\mathbf{x}+\mathbf{e}_i\delta_t, t+\delta_t) = I_i(\mathbf{x},t) - \frac{\delta_t}{\tau_I}\left[I_i(\mathbf{x},t) - I_i^{(eq)}(\mathbf{x},t)\right] \tag{12}$$

where τ_I is the relaxation time. The equilibrium particle distribution function $I_i^{(eq)}$ is $I_i^{(eq)} = \sum_{i=1}^{Q} I_i w_{gi}$. $w_{gi} = \frac{\Delta\delta_i}{2\pi}$ is the weighted coefficient corresponding to the discrete direction i. δ_i is the azimuthal angle. The incoming unknown particle distribution functions are computed from the knowledge of the boundary temperature, and for a black boundary, they are given by $I_i = \frac{\sigma_{SB}T_{bound}^4}{\pi}$. σ_{SB} is the Stefan-Boltzmann constant. T_{bound} is the boundary temperature.

Once the droplet starts to be frozen, the droplet will have no deformation. To more accurately simulate the freezing process of a falling droplet, the solid volume fraction is used to modify the migration step of the evolution equation. The modified migration equation is:

$$f_i(\mathbf{x}, t+\delta_t) = \alpha_s f_i^*(\mathbf{x},t) + (1-\alpha_s)f_i^*(\mathbf{x}-\mathbf{e}_i\delta_t, t) \tag{13}$$

where f_i^* is the particle distribution function after the collision process. For $\alpha_s = 0$, the migration step is the same as the original one, and the particle at a given node completely moves to its neighbor node. For $\alpha_s = 1$, the particle at a given node does not migrate. For $0 < \alpha_s < 1$, a fraction of the particle at a given node moves to its neighbor node.

The density is $\rho(\mathbf{x},t) = \sum_{i=0}^{8} f_i(\mathbf{x},t)$, the velocity is $\mathbf{u}(\mathbf{x},t) = (\sum_{i=0}^{8} f_i(\mathbf{x},t)\mathbf{e}_i + \frac{\delta_t}{2}\sum_{i=0}^{8}\mathbf{F}(\mathbf{x}))/\rho(\mathbf{x},t)$ and the temperature is $T(\mathbf{x},t) = \sum_{i=0}^{8} g_i(\mathbf{x},t)$. The flowchart of the solution procedure is shown in Figure 1.

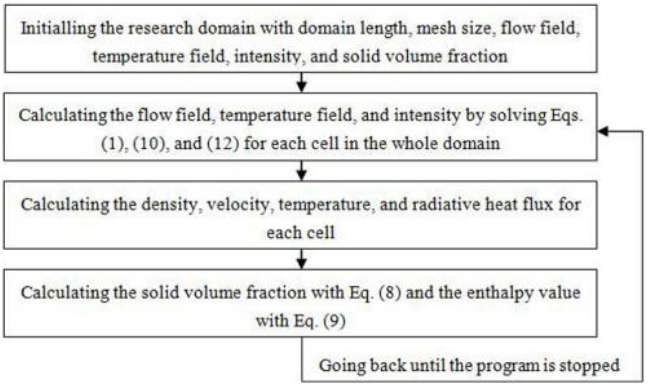

Figure 1.
Flowchart of the solution procedure

3. Freezing process of a falling droplet

3.1 Validation test

3.1.1 Solidification from a corner in a quarter-space. To show the correctness of the present LBM, the solidification from a corner in a quarter-space is performed. Initially, all the space is filled with liquid at a uniform temperature $T_i = 0.3$. The temperature at the west and south boundary is $T_O = -1.0$ for time $t \geq 0$.The nucleation temperature is $T_n = 0.0$. Figure 2 shows the temperature distribution and solid volume fraction at time step $t = 2{,}000$. It can be seen that the temperature is gradually reduced along the northeast corner to the southwest corner. The simulation results are compared with the analytical solutions presented by Rathjen and Jiji (1971). The analytical solution of the interface position is:

$$0 = -1 + \left(1 + T_{in}^{*}\right) erf(x^{*}) erf\left(f(x^{*})\right) + \frac{\beta}{2\pi}\int_0^1 \int_{x_0^{*}}^{\Lambda} \left[f(\eta) - \eta \frac{df(\eta)}{d\eta}\right] \times \left[\mathrm{K}(\eta, \tau, x^{*})\mathrm{K}\left(f(\eta), \tau; f(x^{*})\right) + \mathrm{K}\left(f(\eta), \tau; x^{*}\right)\mathrm{K}\left(\eta, \tau; f(x^{*})\right)\right] d\eta \frac{d\tau}{1-\tau} + \frac{\beta\lambda}{4\pi^{1/2}}\int_0^1 \left[\mathrm{K}(\lambda, \tau; f(x^{*}))\mathrm{K}(\tau; \Lambda; x^{*}) + \mathrm{K}(\lambda, \tau; x^{*})\mathrm{E}(\tau; \Lambda; f(x^{*}))\right] \frac{d\tau}{\tau^{1/2}(1-\tau)^{1/2}} \tag{14}$$

where T^{*} is the dimensionless initial temperature. x^{*} is the dimensionless coordinate. β is the ratio of latent heat to sensible heat. x_0^{*} is the intersection of line $y^{*} = x^{*}$ and interface curve in x^{*}, y^{*} domain. η is the integration variable. τ_0 is the integration variable. λ_0 is a constant in one-dimensional solution–stationary interface position. Λ is a dimensionless constant such that $f(x^{*} > \Lambda) \approx \lambda_0$. For solving this equation, some mathematical methods are introduced, and then the interface curve function is:

$$f(x^{*}) = \left[\lambda_0{}^{m} + \frac{C}{x^{*m} - \lambda_0^{m}}\right]^{1/m} \tag{15}$$

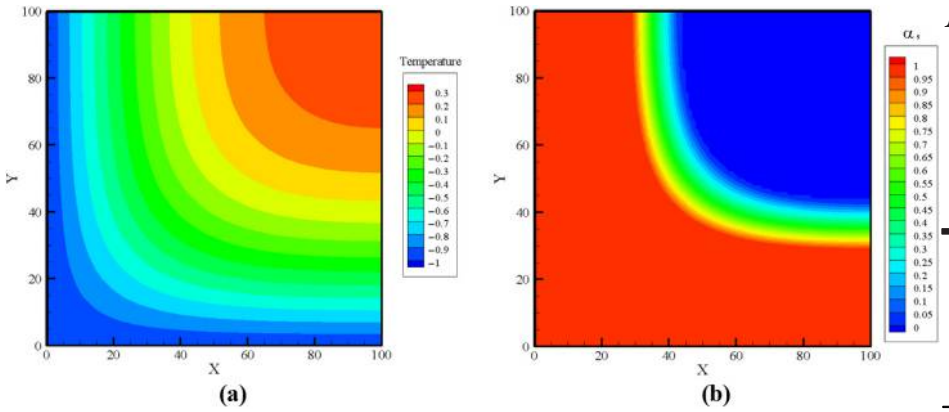

Figure 2. Temperature distribution and (a) solid volume fraction α_s (b) at time step $t = 2000$

where $f(x^*)$ is the interface curve function. C and m are determined through $f(x_0^*) = x_0^*$ and $f(x_1^*) = (x_0^* + \lambda_0)/2$, respectively. The detailed solution process is given in Rathjen and Jiji (1971). Figure 3 shows the comparison results for the solid–liquid interfacial position. It can be seen that the simulation results and the analytical solutions are in good agreement.

3.1.2 Radiation in a 2D square geometry. To show the compatibility of the lattice Boltzmann formulation for the radiation problem, a transient conduction and radiation in a 2D square geometry is performed. Initially, the entire system is at temperature $T_N = T_W = T_E = 0.5$. For $t > 0$, the south boundary temperature is raised to $T_S = 1.0$. The enclosed gray-homogeneous medium is absorbing, emitting and isotropically scattering. The extinction coefficient is 1.0. The lattice is 20×20. In Figure 4, the temperatures at three locations along the centerline ($x/X = 0.5$) are compared with those reported in the literature (Wu and Ou, 1994; Yuen and Takara, 1988). It is seen that the simulation results of the lattice Boltzmann formulation are compared very well with those reported in the literature.

3.1.3 Freezing process of a droplet in a gas steam. The present model is used to simulate the freezing process of a droplet in a gas steam in reference (Liao and Ng, 1990) to illustrate

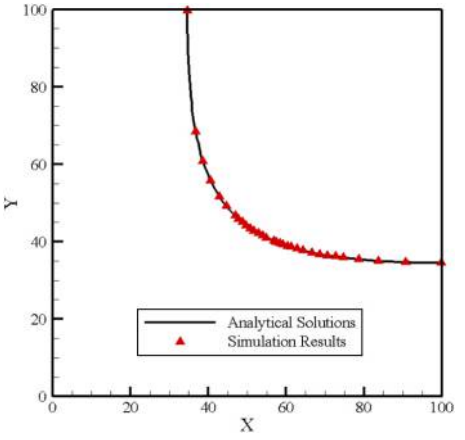

Figure 3. Comparison results for the solid–liquid interfacial position between simulation results and analytical solutions

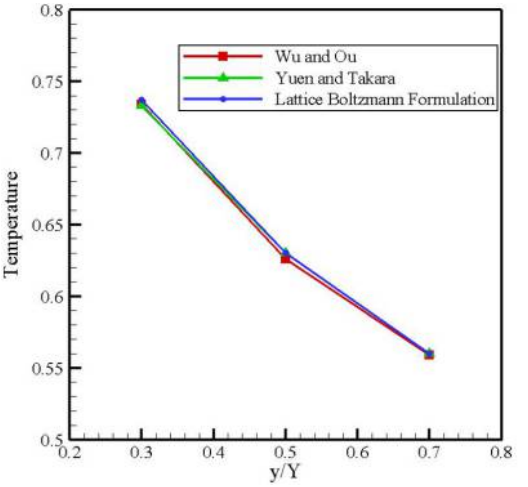

Figure 4.
Comparison of steady-state centerline ($x/X = 0.5$) temperature at three locations in a black square enclosure

its correctness. Figure 5 gives the comparison results of the LBM numerical results and analytical solutions for the solid fraction in a droplet as a function of droplet diameter at time $t = 0.06$ s. The analytical solutions of the solid fraction W_s/W_D are $W_s/W_D = \frac{c_p}{L_s} e^{\frac{Ah}{W_D c_p} t} t$. Where L_s is the latent heat of freezing of water. A is the surface area of the droplet. W_D is the total weight of the droplet. It can be concluded that the relative error of the simulation results and the analytical solutions is less than 5 per cent. In other words, good agreements with the analytical solutions and simulation results are achieved. Therefore, the freezing process of a falling droplet can be well simulated by using the modified enthalpy-based LBM.

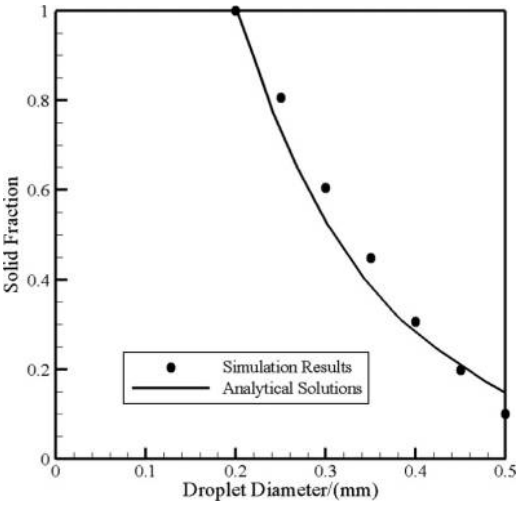

Figure 5.
Relationship of the solid fraction and the droplet diameter at time $t = 0.06$ s

3.2 Simulation model

In this study, the conversion method of the lattice units and physical units is the dimensional analysis method. Here, a computed domain of 0.03 × 0.07 m is used. The dimension of the lattice is 600 × 1400. Initially, there is a droplet with temperature of $T_{l,in}$ = 273 K in a cold space. The initial droplet diameter is D = 0.003 m. The droplet density is ρ_l = 1000 kg/m^3. The initial vertical velocity is $v0$ = 0.001 m/s. The initial cold space temperature is $T_{g,in}$ = 223 K. The nucleation temperature is T_n = 268 K. Figure 6 gives the computed domain about the freezing process of a falling droplet in a cold space. The periodic boundary scheme with second-order accuracy is used at the walls of the domain (Chen *et al.*, 1996). In this case, the specific heat capacity ratio of liquid and solid is c_p: c_{solid} = 2:1. The viscosity ratio of liquid and gas is v_l: v_g = 1:1.The latent heat of phase change is $L = 20 \times 10^{-3}$ J/kg. The thermal conductivity is k = 0.55 W/(m·K). The Prandtl number is Pr = 0.71.

3.3 Mesh independence

First, the mesh independence is checked, five sets of grids at different sizes (gird 1: 150 × 350, gird 2: 300 × 700, gird 3: 600 × 1400, gird 4: 750 × 1750, gird 5: 900 × 2100) are considered. Figure 7 shows the variation of the solid volume fraction at point A for different grids

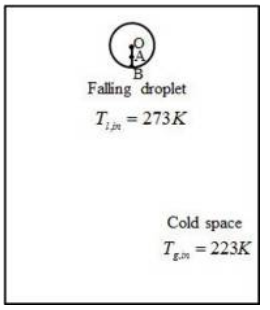

Figure 6.
Computed domain about the freezing process of a falling droplet (point O is the center of the droplet, point B is the boundary of the droplet and point A is the midpoint of point O and point B)

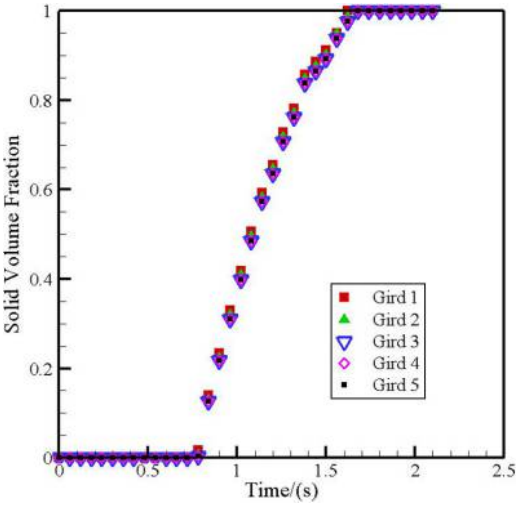

Figure 7.
Variation of the solid volume fraction at point A in different grid systems

system. It can be found out that the relative error between grid 3, grid 4 and grid 5 is less than 0.1 per cent, so in view of calculation cost, grid 3 will be used for simulation.

3.4 Results and discussions

3.4.1 Temperature and solid volume fraction. For the case in Section 3.2, the temperature field and streamlines in a cold space at different time are shown in Figure 8. Figure 9 gives

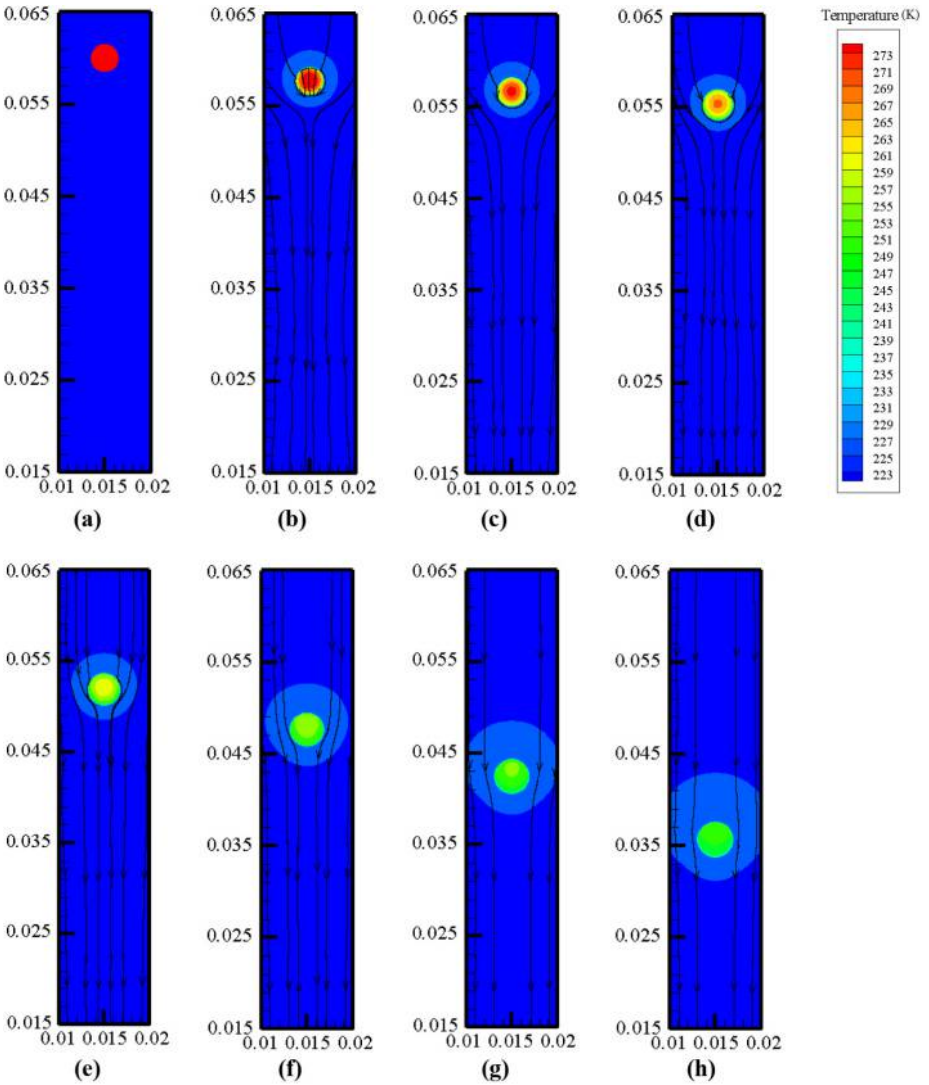

Figure 8.
Temperature field and streamlines in a cold space at different times

Notes: (a) t = 0 s; (b) t = 0.6 s; (c) t = 0.75 s; (d) t = 0.9 s; (e) t = 1.2 s; (f) t = 1.5 s; (g) t = 1.8 s; (h) t = 2.22 s

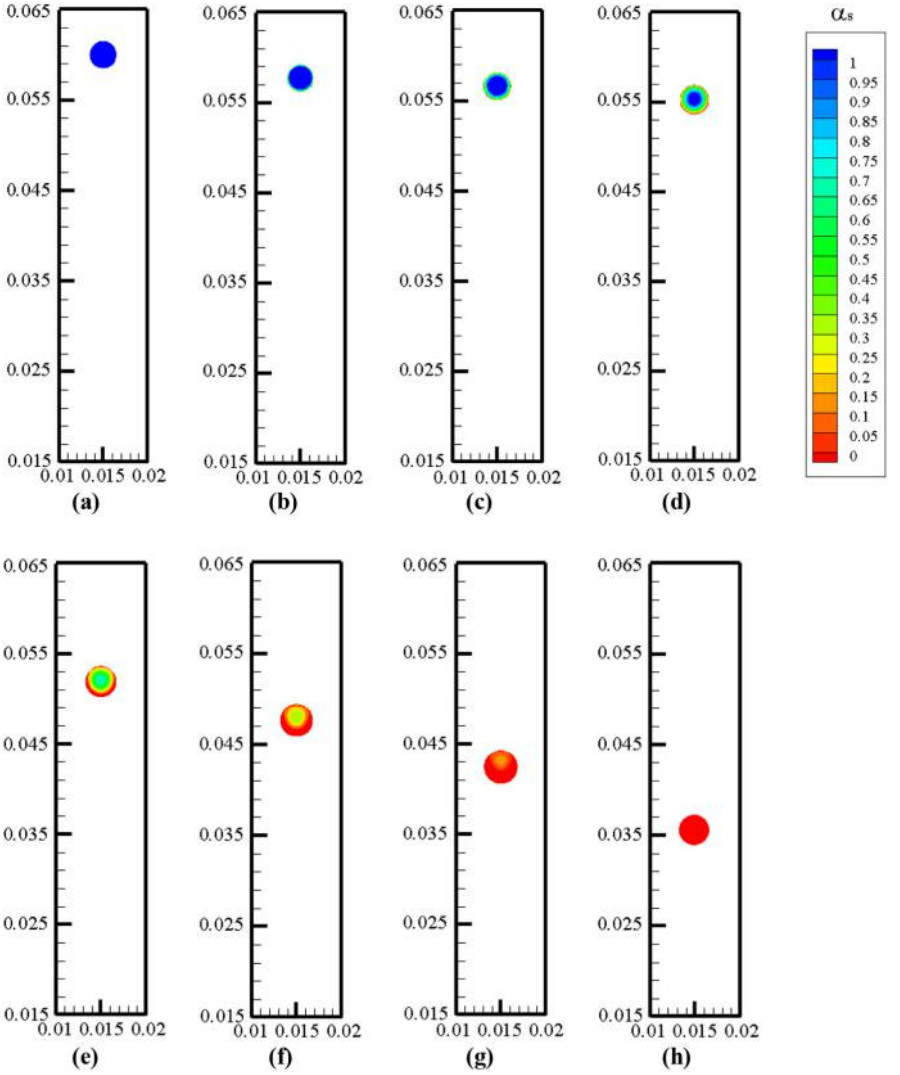

Notes: (a) t = 0 s; (b) t = 0.6 s; (c) t = 0.75 s; (d) t = 0.9 s; (e) t = 1.2 s; (f) t = 1.5 s; (g) t = 1.8 s; (h) t = 2.22 s

Figure 9.
Solid volume fraction of a falling droplet in a cold space at different time

that the solid volume fraction distribution of the droplet in different time. Based on the above results, the freezing process can be summarized as follows: the droplet falls in a cold space. Meanwhile, it is cooled by the external gas. Due to the heat conduction, the droplet temperature decreases as time goes. When the droplet temperature is reduced below the nucleation temperature, the droplet begins to be frozen. For the whole droplet, the freezing process first occurs at the surface (as shown in Figure 9(c)). Then, the liquid–solid interface

of the droplet gradually moves toward the center until the droplet is completely frozen into an ice particle (as shown in Figure 9(c)-(h)). However, it can be seen that the solid volume fraction distribution of droplet is asymmetric in the late stage of the falling process, which indicates that the lower part of the droplet is frozen earlier than the upper part (as shown in Figure 9(f)). It is because that the cooling effect of air in the lower part is stronger than that in the upper part. In addition, the fluid flow around the droplet also has an effect on the flow field. The variation of flow field can lead to uneven temperature distribution.

In the present study, the solid volume fraction value of the droplet is obtained which can be used to forecast the freezing time. The solid volume fraction from point O to point B at time $t = 0.75$ and $t = 1.2$ s are shown in Figure 10. The solid volume fraction of the droplet surface is higher than that of the droplet center.

Figure 11 expresses the solid volume fraction increment of point O and point B in droplet at the same time interval. It illustrates that the increment of solid volume fraction increases first, and then decreases at point B and point O. In other words, the freezing trend eventually

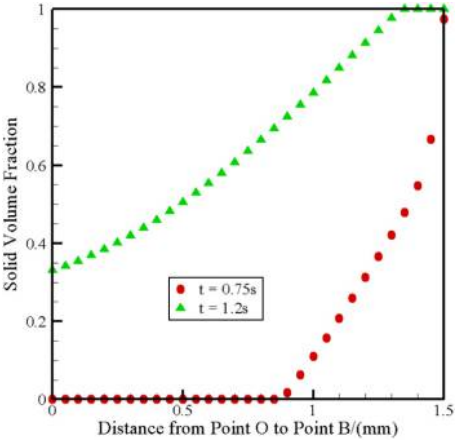

Figure 10.
Solid volume fraction of a falling droplet from point O to point B at $t = 0.75$ s and $t = 1.2$ s

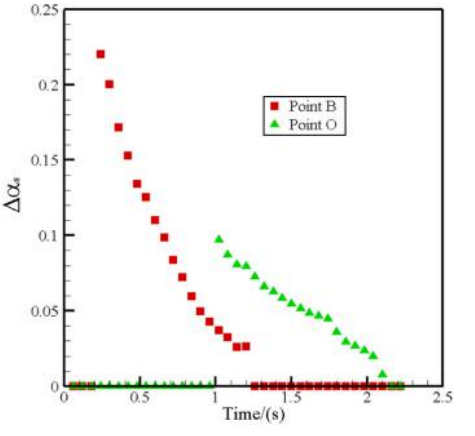

Figure 11.
Solid volume fraction increment of point O and point B in droplet at the same time interval

slows down in the later stage of the freezing process. When the droplet is fully frozen into an ice particle, the increment of solid volume fraction in the whole droplet completely becomes zero.

3.4.2 Droplet shape. During the droplet falling in a cold space, its shape has changed. When the freezing process of a droplet takes place, an ice shell is formed to hinder the droplet deformation. Then, the droplet keeps on falling and has no deformation. The initial vertical velocity and nucleation temperature are the main effect factors of this phenomenon.

3.4.2.1 Initial vertical velocity. Figure 12(a) shows that the relationship of the ratio of the largest axis to the smallest axis in the droplet and time at different initial vertical velocities (from v_0 = 0.001 m/s to v_0 = 0.02 m/s). It can be seen that the droplet shape has a significant deformation at the larger initial vertical velocity. It is because that the droplet in larger initial vertical velocity has a bigger resistance.

3.4.2.2 Nucleation temperature. Figure 12(b) indicates that the relationship of the ratio of the largest axis to the smallest axis in the droplet and time at different nucleation temperature (from T_n = 270 K to T_n = 259 K). It is illustrated that the droplet shape obviously changes when the nucleation temperature is lower. The mainly reason is that the droplet falls longer time and has more time to change at the lower nucleation temperature.

3.4.3 Freezing time. Freezing time is an important factor for studying the freezing process which determines the freezing efficiency. In this section, the freezing time as a function of (1) nucleation temperature, (2) initial temperature and (3) droplet diameter are simulated. Figure 13(a) presents the relationship between the nucleation temperature and freezing time at a certain droplet size. It is demonstrated that the freezing time decreases along with the nucleation temperature increases. Figure 13(b) gives the initial temperature as a function of freezing time at a certain droplet size which is indicated that the freezing time increases as the initial temperature increases. They are mainly due to the effect of nucleation driving force, because the nucleation driving force becomes higher when the nucleation temperature increases or the initial temperature deceases. The higher nucleation driving force promotes the nucleation phenomenon occurring earlier. Hence, the freezing time is shortened. In practical production, the nucleation temperature can be improved by adding nucleators, and the

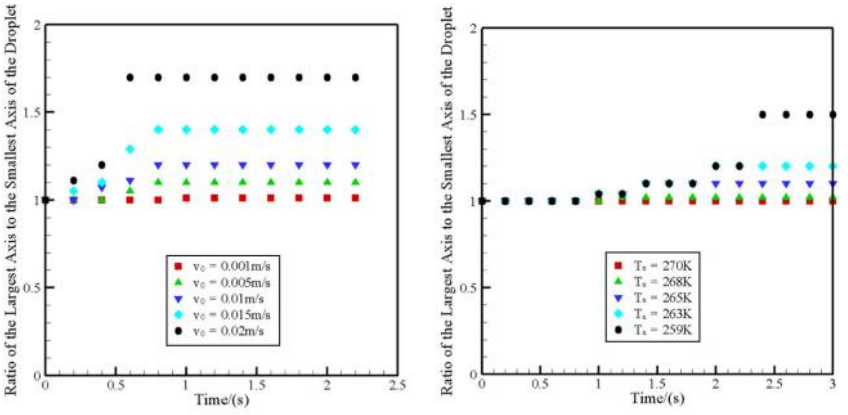

Notes: (a) Initial vertical velocities; (b) nucleation temperature

Figure 12. Relationship of the ratio of the largest axis to the smallest axis in droplet and different time

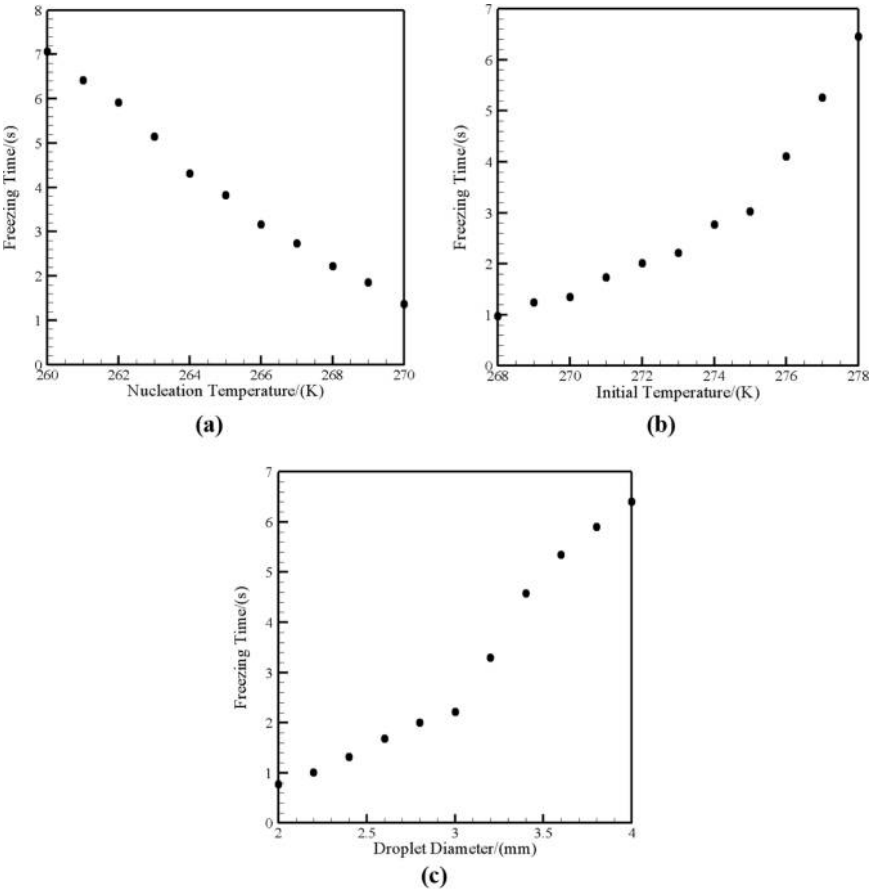

Figure 13.
Relationship of (a) nucleation temperature, (b) initial temperature, (c) droplet diameter and freezing time

initial temperature can be decreased by prolonging the cooling time. The freezing time as a function of droplet diameter at a certain nucleation temperature is shown in Figure 13(c). It is declared that the freezing time increases when the droplet diameter increases. The primarily reason is both the decreased surface area per unit weight and increased terminal velocity as the droplet size increases. However, in practical

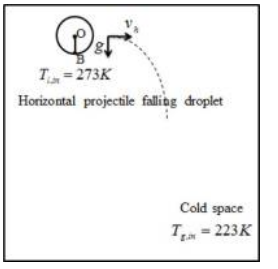

Figure 14.
Physical model about the freezing process of a falling droplet with initial horizontal velocity

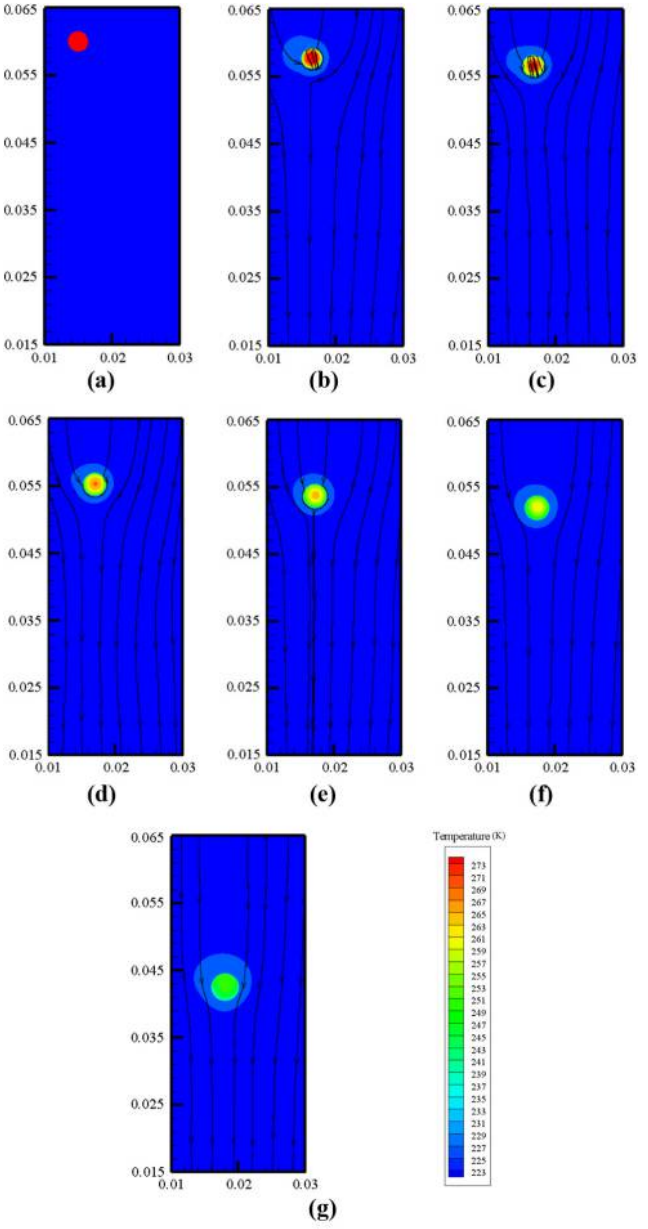

Notes: (a) t = 0 s; (b) t = 0.6 s; (c) t = 0.75 s; (d) t = 0.9 s; (e) t = 1.05 s; (f) t = 1.2 s; (g) t = 1.8 s

Figure 15.
Temperature field and streamlines in a cold space at different times

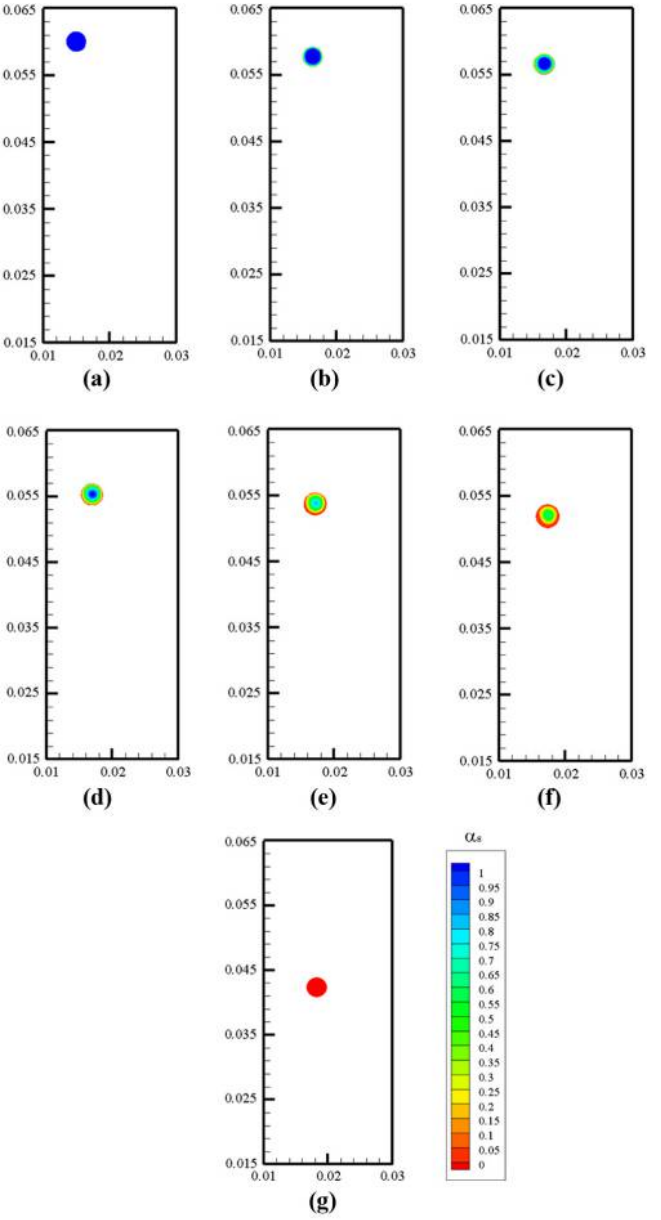

Figure 16.
Freezing process of a falling droplet with initial horizontal velocity

Notes: (a) t = 0 s; (b) t = 0.6 s; (c) t = 0.75 s; (d) t = 0.9 s; (e) t = 1.05 s; (f) t = 1.2 s; (g) t = 1.8 s

applications (e.g. artificial snowmaking), sometimes, if the droplet diameter is too small, the droplet will be blown away by the wind due to its small terminal velocity. Therefore, it is favorable to raise the freezing efficiency of a falling droplet in a cold space by altering the initial temperature or the nucleation temperature.

4. Freezing process of a falling droplet with initial horizontal velocity

In this section, when a droplet falls in a cold space, the influence of initial horizontal velocity is studied. Figure 14 expresses the distribution diagrams about the freezing process of a falling droplet with initial horizontal velocity. A constant initial horizontal velocity (v_h = 0.003 m/s) is given. The computational domain is 0.05 × 0.07 m. The dimension of the lattice is 1000 × 1400. Other conditions are identical to those of Figure 6. Figure 15 explains that temperature field and streamlines in a cold space at different time. Figure 16 shows that the solid volume fraction of a falling droplet with initial horizontal velocity at different time. It is apparent that the droplet falls in a cold space under the effect of the initial vertical velocity, gravity and initial horizontal velocity. The solid volume fraction distribution of the droplet is asymmetric at the later stage of the falling process, which indicates that the lower part of the droplet is frozen earlier than the upper part of the droplet (as shown in Figure 16(e)-(f)). To further illustrate this phenomenon, the local enlarged image of the freezing droplet for freezing processes of a falling droplet without and with initial horizontal velocity in time t = 1.2 s are shown in Figure 17. One important argument for this phenomenon is that the cooling effect of air in the lower part is stronger than in the upper part. Meanwhile, the cooling effect in the lower part is better than that in the upper part due to the influence of flow field.

Obviously, the droplet shape is influenced by the initial horizontal velocity before freezing occurs. Figure 18 shows the relationship of the ratio of the largest axis to the smallest axis in the droplet and time at different initial horizontal velocities (from v_h = 0.001 m/s to v_h = 0.01 m/s). It can be demonstrated that the droplet shape evidently changes at the larger horizontal velocity. The main reason is that the distribution of flow field around the droplet makes it deformed before freezing.

The freezing time is affected by the initial horizontal velocity as shown in Figure 19. It can be seen that the freezing time decreases at larger initial horizontal velocity, because the heat transfer increases as the initial horizontal velocity is increased.

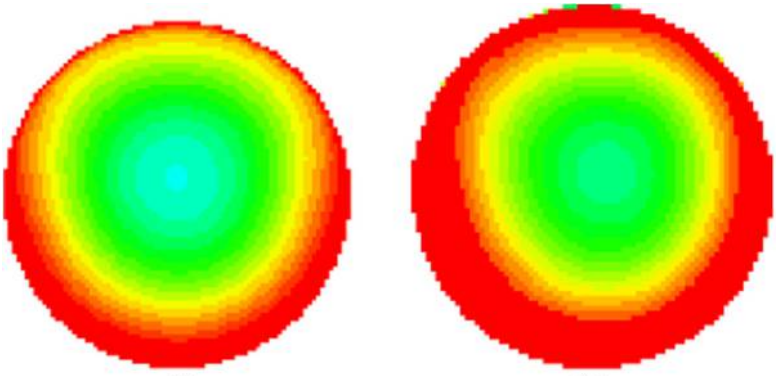

Notes: (a) Without initial horizontal velocity; (b) with initial horizontal velocity

Figure 17. Local enlarged image of the freezing droplet for freezing processes of a falling droplet without and with initial horizontal velocity in time t = 1.2 s

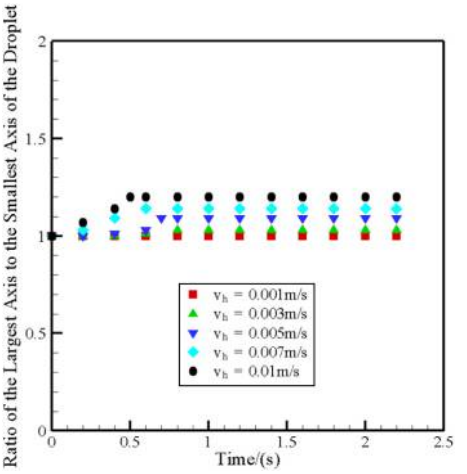

Figure 18.
Relationship of the ratio of the largest axis to the smallest axis in droplet and time at different horizontal velocities

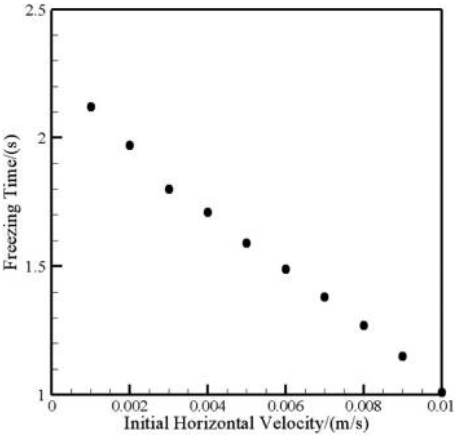

Figure 19.
Relationship of the initial horizontal velocity and the freezing time at a certain droplet size

5. Conclusions

The freezing processes of a falling droplet without and with initial horizontal velocity have been studied by a modified enthalpy-based LBM. In the present model, the improved pseudo-potential model is used and the radiation is considered. First, three cases are carried out to validate the accuracy of the present model, which gives a good qualitative validation of the modeling. Second, the freezing process of a falling droplet in a clod space is simulated. The temperature field, streamlines and solid volume fraction of the droplet are investigated. The simulation shows that the lower part of the droplet is firstly frozen due to the stronger cooling effect of air in the lower position and flow field. However, for the whole droplet, the freezing firstly occurs at the surface. Furthermore, the increment of solid volume fraction from the droplet center to the edge is acquired. The freezing trend slows down in the later stage of the freezing process. In addition, the impacts of the initial vertical velocity and

nucleation temperature on the droplet deformation are obtained. It is demonstrated that the droplet is deformed from ball to oval before the ice shell forms. Moreover, the effect factors of the freezing time for a falling droplet are studied numerically. Finally, the freezing process of a falling droplet with initial horizontal velocity is simulated. The lower part of the droplet is frozen earlier than the upper part of the droplet, because the cooling effect of air in lower part is stronger than that in the upper part and the temperature distribution is influenced by the flow field. It is evidenced that the droplet shape is in relation to the initial horizontal velocity. Additionally, the freezing time is decreased when the initial horizontal velocity is larger. In the present study, the falling droplet in a cold space is simulated at the situation of low Ma number.

References

Anandharamakrishnan, C., Gimbun, J., Stapley, A.G.F. and Rielly, C.D. (2009), "Application of computational fluid dynamics (CFD) simulations to spray-freezing operations", *Drying Technology*, Vol. 28 No. 1, pp. 94-102.

Asinari, P., Mishra, S.C. and Borchiellini, R. (2010), "A lattice Boltzmann formulation for the analysis of radiative heat transfer problems in a participating medium", *Numerical Heat Transfer, Part B: Fundamental*, Vol. 57 No. 2, pp. 126-146.

Chen, S., Martinez, D. and Mei, R. (1996), "On boundary conditions in lattice Boltzmann methods", *Physics of Fluids*, Vol. 8 No. 9, pp. 2527-2536.

Du, P., Hu, H., Ren, F. and Song, D. (2017), "Bubble characterizations on hydrophobic surface using lattice Boltzmann simulation with large density ratios", *International Journal of Numerical Methods for Heat and Fluid Flow*, Vol. 27 No. 6, pp. 1311-1322.

Gao, P., Cheng, B., Zhou, X., Zhang, D. and Zhou, G. (2016), "Study on droplet freezing characteristic by ultrasonic", *Heat and Mass Transfer*, Vol. 1, pp. 1-10.

Hallett, J. (1964), "Experimental studies of the crystallization of supercooled water", *Journal of the Atmospheric Sciences*, Vol. 21 No. 6, pp. 671-682.

Hindmarsh, J.P., Russell, A.B. and Chen, X.D. (2007), "Fundamentals of the spray freezing of foods – microstructure of frozen droplets", *Journal of Food Engineering*, Vol. 78 No. 1, pp. 136-150.

Hindmarsh, J.P., Buckley, C., Russell, A.B., Chen, X.D., Gladden, L.F., Wilson, D.I. and Johns, M.L. (2004), "Imaging droplet freezing using MRI", *Chemical Engineering Science*, Vol. 59 No. 10, pp. 2113-2122.

Hobbs, P.V. and Alkezweeny, A.J. (1968), "The fragmentation of freezing water droplets in free fall", *Journal of the Atmospheric Sciences*, Vol. 25 No. 5, pp. 881-888.

Huang, J. and Bartell, L.S. (1995), "Kinetics of homogeneous nucleation in the freezing of large water clusters", *The Journal of Physical Chemistry*, Vol. 99 No. 12, pp. 3924-3931.

Jeffery, C.A. and Austin, P.H. (1997), "Homogeneous nucleation of supercooled water: results from a new equation of state", *Journal of Geophysical Research: Atmospheres*, Vol. 102 No. D21, pp. 269-275.

Jiaung, W.S., Ho, J.R. and Kuo, C.P. (2001), "Lattice Boltzmann method for the heat conduction problem with phase change", *Numerical Heat Transfer: Part B: Fundamentals*, Vol. 39 No. 2, pp. 167-187.

Krämer, B., Hübner, O., Vortisch, H. and Baumgärtel, H. (1999), "Homogeneous nucleation rates of supercooled water measured in single levitated microdroplets", *The Journal of Chemical Physics*, Vol. 111 No. 14, pp. 6521-6527.

Liao, J.C. and Ng, K.C. (1990), "Effect of ice nucleators on snow making and spray freezing", *Industrial and Engineering Chemistry Research*, Vol. 29 No. 3, pp. 361-366.

López, M.L. and Ávila, E.E. (2012), "Deformations of frozen droplets formed at−40° C", *Geophysical Research Letters*, Vol. 39 No. 1, pp. 1-5.

Miller, R.C., Anderson, R.J. and Kassner, J.L. Jr. (1976), "Evaluation of the classical theory of nucleation using expansion chamber measurements of the homogeneous nucleation rate of water from the vapor", *Colloid and Interface Science: Aerosols, Emulsions, and Surfactants*, Vol. 2, Academic Press, Cambridge, MA, pp. 1-21.

Miller, W., Rasin, I. and Succi, S. (2006), "Lattice Boltzmann phase-field modelling of binary alloy solidification", *Physical A: Statistical Mechanics and its Applications*, Vol. 362 No. 1, pp. 78-83.

Nagumo, N. and Fujiyoshi, Y. (2015), "Microphysical properties of slow-falling and fast-falling ice pellets formed by freezing associated with evaporative cooling", *Monthly Weather Review*, Vol. 143 No. 11, pp. 4376-4392.

Rathjen, K.A. and Jiji, L.M. (1971), "Heat conduction with melting or freezing in a corner", *Journal of Heat Transfer*, Vol. 93 No. 1, pp. 101-109.

Shan, X. and Chen, H. (1994), "Simulation of nonideal gases and liquid-gas phase transitions by the lattice Boltzmann equation", *Physical Review E*, Vol. 49 No. 4, p. 2941.

Wood, S.E., Baker, M.B. and Swanson, B.D. (2002), "Instrument for studies of homogeneous and heterogeneous ice nucleation in free-falling supercooled water droplets", *Review of Scientific Instruments*, Vol. 73 No. 11, pp. 3988-3996.

Wu, C.Y. and Ou, N.R. (1994), "Transient two-dimensional radiative and conductive heat transfer in a scattering medium", *International Journal of Heat and Mass Transfer*, Vol. 37 No. 17, pp. 2675-2686.

Yuen, W.W. and Takara, E.E. (1988), "Analysis of combined conductive-radiative heat transfer in a two-dimensional rectangular enclosure with a gray medium", *Journal of Heat Transfer*, Vol. 110 No. 2, pp. 468-474.

Zarghami, A., Ubertini, S. and Succi, S. (2014), "Finite volume formulation of thermal lattice Boltzmann method", *International Journal of Numerical Methods for Heat and Fluid Flow*, Vol. 24 No. 2, pp. 270-289.

Zhao, X., Dong, B., Li, W. and Dou, B. (2017), "An improved enthalpy-based lattice Boltzmann model for heat and mass transfer of the freezing process", *Applied Thermal Engineering*, Vol. 111 No. 25, pp. 1477-1486.

Corresponding author
Bo Dong can be contacted at: bodong@dlut.edu.cn